Hydrology and
Earth System
Sciences
Discussions

EGU

Open Access

Hydrological Signals in Tilt and Gravity Residuals at Conrad Observatory (Austria)

Bruno Meurers[1], Gábor Papp[2], Hannu Ruotsalainen[3], Judit Benedek[2], Roman Leonhardt[4]

[1] University of Vienna, Department of Meteorology and Geophysics, 1090 Wien, Austria
5 [2] Geodetic and Geophysical Institute, Research Centre for Astronomy and Earth Sciences, Hungarian Academy of Sciences, 9400 Sopron, Hungary
[3] Finnish Geospatial Research Institute, FGI, National Land Survey of Finland, 02430 Masala, Finland
[4] Zentralanstalt für Meteorologie und Geodynamik (ZAMG), 1190 Wien, Austria

Correspondence to: Bruno Meurers (bruno.meurers@univie.ac.at)

10 **Abstract.** The Superconducting Gravimeter GWR C025 monitors the vertical component of the gravity vector at the Conrad Observatory (Austria) since autumn 2007. Two tilt meters operate continuously since spring 2016: a 5.5m long interferometric water level tilt meter and a Lippmann-type 2D pendulum tilt sensor. The co-located and co-oriented set up enables a wide range of investigations because tilts are sensitive both to geometrical solid Earth deformations and to gravity potential changes. The tide free residuals of the SG and both tilt meters clearly reflect the gravity/deformation effects
15 associated with short- and long-term environmental processes and reveal a complex water transport process at the observatory site. Water accumulation on the terrain surface causes short-term (a few hours) effects which are clearly imaged by the SG gravity and N-S tilt residuals. Long-term (> a few days/weeks) tilt and gravity variations occur frequently after long-lasting rain, heavy rain or rapid snowmelt. Gravity and tilt residuals are associated to the same hydrological process but have different physical causes. SG gravity residuals reveal the gravitational effect of water mass transport, while modelling
20 results exclude a purely gravitational source of the observed tilts. Tilt residuals show the response on surface loading instead. N-S tilt signals are much stronger than those of the E-W component most probably due to the well-known cavity effect of the 150 m long tunnel oriented in E-W direction.

1 Introduction

The gravity field of the Earth changes temporally mainly because of external forcing, but also due to direct gravitational and
25 indirect effects of mass transport in the entire Earth system. This happens in all spatial and temporal scales, from local to global and from very short-term to secular gravity variations. Mass transport does not only change the density distribution which directly affects the gravity potential, but is mostly associated with deformation processes caused by loading. Today, superconducting gravimeters (SG) are the most sensitive instruments for monitoring the temporal variation of the magnitude of the gravity vector. They provide highly accurate gravity time series reflecting various geodynamical phenomena like
30 Earth tides, Earth rotation, normal modes and environmental (including hydrological) gravity effects (e.g. Hinderer et al.,

2007). Gravimeter signals are dominated by the vertical component of the gravity vector, tilt meter signals by the horizontal component as well as by rotation of the tilt meter base with respect to the plumb line. In the latter case local effects can play an important role, because tilt is affected by the topography and by geometry and size of the cavity where the tilt meters are installed (e.g. Agnew, 1986).

35   The Central Institute for Meteorology and Geodynamics (ZAMG, Austria) operates the Superconducting Gravimeter (SG) GWR-C025 since 1995 within the framework of the Global Geodynamics Project (GGP, Crossley et al., 1999) and later the International Geodynamics and Earth Tide Service (IGETS, Voigt et al., 2016). After terminating a gravity time series at Vienna (Austria) extending over 12 years, the SG was moved to the Conrad observatory (CO, Austria) in autumn 2007, starting a gravity time series over 11 years that lasted until November 2018.

40   Looking at the non-tidal contribution to gravity variations revealed a much larger hydrological impact on the time series at CO than at Vienna obviously due to complex water infiltration processes taking place after long-lasting rain or rapid snow melt (Mikolaj and Meurers, 2013). Such events cause long-term (a few weeks) residual features the source of which could not be unambiguously identified so far. The installation of two tilt meters in 2014 provided new insight into possible scenarios of hydrological water transport at CO by comparing tide-free SG and tilt time-series which is subject of the
45   investigation reported subsequently.

2 Observation site and instrumentation

The Conrad observatory is a geophysical/geodynamic research facility located 60 km SW of Vienna (Austria) in a carbonate region belonging to the Eastern foothill of the Eastern Alps, close to the top of mountain Trafelberg in 1050 m altitude. The Trafelberg Mountain itself is part of the Northern Calcareous Alps and shows a complicated nappe-structure consisting of
50   Main Dolomite and Wetterstein/Gutenstein limestone (Blaumoser, 2011; Bryda and Posch-Trözmüller, 2015). Three karstic caves are known in the wider surroundings of the observatory (Hartmann and Hartmann, 2000). No natural springs exist on Trafelberg itself (Deisl et al., 2013). Therefore karstic phenomena like complex underground drainage systems, karst aquifers, caves and cavern systems, as well as sinkholes are expected to be present.

The SG is located in a separate laboratory in the front part of the observatory (Fig. 1). Gravity data are sampled with 1 Hz by
55   two redundant digital volt meters (DVM) for detecting possible long-term scale factor changes of the DVMs. SG calibrations by co-located absolute gravimeter (JILAg-6, FG-5) observations took place twice a year, supported by numerous SG/Scintrex CG-5 relative gravimeter intercomparisons (Meurers, 2012; Meurers, 2018a). Commonly, the SG scale factor (SF) is assumed to remain constant as long as the hardware (e.g. coil geometry, transfer function) does not change (Goodkind, 1999) which allows for averaging the calibration results (Crossley et al., 2018). Systematic SF changes, if
60   present and larger than 0.1-0.2‰, are reliably detectable by studying the temporal M2 tidal parameter modulation of successive tidal analyses over 1 yr intervals. Combing calibration results and M2 parameter modulation studies (Meurers et al., 2016) proved the accuracy and time-stability of the SG scale factor at CO to be far below 1‰ (Meurers, 2018a).

In August 2014, the Geodetic and Geophysical Institute (GGI Sopron, Hungary) installed a 5.5 m long one end Michelson-Gale type interferometric water level tilt meter (iWT) at CO, designed by the Finnish Geodetic Institute (FGI) (Ruotsalainen
65 et al., 2016a; 2016b; Ruotsalainen, 2018). Continuous tilt measurements started at CO in order to monitor geodynamical phenomena like microseisms, free oscillations of the Earth, earth tides, mass loading effects (ocean tidal and atmospheric loading) and possible crustal deformations. In July 2015, a Lippmann HRTM 2D tilt sensor (LTS) with <1 nrad resolution (https://www.l-gm.de/en/en_tiltmeter.html) was installed by GGI close to the iWT on the same 6 m long pier (Papp et al., 2019). This setup of instruments based on different physical principles (relative height change of a level surface vs.
70 inclination change of the plumb line) allows for comparing the response of tilt meters with long (several meters) and short (a few decimetres) base length. The maximum crustal movement in one end of the tilt meter estimated by theoretical earth tide tilt is 0.7 x 250 nrad = 175 nrad, which is 175 nm tilt / 1m base, 481 nm tilt/ (5.5 m/2 base) and 17.5 nm tilt/(0.2m/2 base) for iWT and LTS respectively. Main disturbing effect is thermal expansion in this kind of instrumentation and an example can be given e.g. for steel used for iWT tube and pot construction. Due to non-linear thermal expansion of water in CO
75 laboratory condition, the linear thermal expansion coefficient of 17 µm/m/K for special stainless steel composition has to be chosen for iWT. This corresponds to 170 nm/m/0.01K, which is the size of tilt movement due to theoretical tidal tilt in 1 m base. We must go beyond 0.01 K temperature stability for the instrument/station requiring very careful thermal isolation. While the current configuration meets the requirements of ongoing research at CO, a two ends interferomeric level tilt meter with a base as long as 50 - 100 m rises the resolution allowing for reliable detection of resonance related signals in the
80 diurnal band and reduces unwanted drift of thermal origin considerably (Ruotsalainen, 2018).

While iWT monitors E-W tilts, LTS provides both N-S and E-W tilt time series. The tilt meter sampling rate is 1Hz (LTS) and 15 Hz (iWT) respectively. The scale factor of the LTS tilt meter is factory based. The iWT scale factor is absolute and based on optical interferometry considering the station condition. The iWT tilt meter detects water level variations as interference phase values which are converted to tilt by a conversion factor based on laser wavelength, refraction coefficient of water and tube length of the tilt meter (Ruotsalainen, 2018). Given the setup at CO (HeNe laser wavelength in air: 542.8
85 nm, refraction coefficient of water under given station conditions: 1.333, tube length: 5.5 m) the conversion factor for the one end iWT system at CO is 74.0 nrad/fringe or 15.26 mas/fringe.

The tilt sensors are installed 94 m apart of the SG in the middle of a 150 m long and 3 m wide tunnel extending E-W. All instruments are underground installations in a thermally stable environment. The front part of the observatory includes the
90 gravimeter laboratory (ceiling height about 4 m) and is covered by gravel up to the tunnel portal. Coverage amounts to approximately 7 m just over the SG. The surroundings of the tunnel consist of solid rocks; the coverage increases towards E from 15 m at the tunnel entrance to about 55 m at the end, with approximately 33 m at the tilt meter site. Based on theoretical calculations by Harrison and Herbst (1977), Bonaccorso et al. (1999) estimate that the maximum amplitude of thermoelastic tilt of the rocks beneath the surface decays towards zero at 10 m depth. Even if this approach might
95 underestimate the real thermoelastic effect as shown by experiments with shallow borehole tilt meters at different depth (Bonaccorso et al., 1999), the coverage of 33 m should reduce thermoelastic tilt deep in the tunnel.

Hydrology and
Earth System
Sciences
Discussions
Open Access
EGU

In order to investigate atmospheric and precipitation effects on gravity, a wide range of meteorological parameters are monitored by mobile and permanent sensors:

100 − air pressure, air temperature, humidity sensors located outside above the laboratory; air pressure sensor included in the SG acquisition system; air pressure, temperature and humidity sensors integrated within the LTS tilt meter housing; additional air pressure and temperature sensors in the observatory labs and the tunnel,

− Tipping bucket rain gauge model AP-23 (Anton Paar) with 0.1 mm resolution,

− Thies disdrometer measuring size and fall speed of precipitation particles and classifying the precipitation type by the SYNOP code,

105 − 3D Thies ultrasonic anemometer.

− SSG-2 snow scale (Sommer Company, Austria) monitoring the weight of the snow pack in front of the observatory and providing snow water equivalent data. The snow scale was out of operation between January 1, 2018 and March 15, 2018. Missing data has been replaced by information from a nearby snow height sensor.

3 Gravity and tilt pre-processing and residual determination

110 For separating small amplitude signals of different physical origin like e.g. hydrological response or tectonic signals we need to subtract tidal effects which dominate the gravity time series. The atmospheric pressure and polar motion are also known to contribute remarkably to temporal gravity and tilt variations although much less than the tides. Both the SG and the tilt meters are relative instruments and hence may exhibit instrumental drift. Generally, the SG drift is expected to be only a few nm/s^2 per year. Absolute gravity observations performed at CO did not reveal significant instrumental drift of the SG until 115 now (Meurers, 2018b). However, the tilt sensors show strong drift dominated by linear trends up to −10 µrad/yr and +2.5 µrad/yr for the LTS and iWT sensors respectively and by possible thermal origin explained above. Therefore, the gravity and tilt time series must be properly processed for deriving residual time series. Pre-processing and determination of gravity/tilt residuals consist of following steps:

120 − Interpolation of 15 Hz iWT data to 5 Hz samples and decimation of 5 Hz data to 1 Hz samples by using a Gaussian operator with 61 coefficients equivalent to 1 min time length.

− Decimation of the 1 Hz data to 1 min samples by applying the numerical FIR filter g1s1m (http://www.eas.slu.edu/GGP/ggpfilters.html).

− Correction of offsets and/or transient signals (tilt sensors only):

125 A) Tilt sensors:

− Removing transient signals due to thermal disturbances in the tunnel which are very small but happen occasionally during maintenance work. Until August 2017, episodic temperature increase as small as a few 0.01°C inside the LTS

Hydrology and
Earth System
Sciences
Discussions
Open Access
EGU

was observed by the built-in sensor, generating tilt signals much larger than the tidal signal. The temperature correction was based on linear or nonlinear models depending on the thermal event. Since August 2017 both tilt sensors are

130   isolated from the temperature fluctuation in the tunnel by styrox-plate insulation.

– Correction of steps, in particular for iWT data, by applying TSOFT (Van Camp and Vauterin, 2005). Due to its incremental measuring principle iWT sometimes suffers from cycle-slip; the correct interpretation of the interferogram phase fails if the phase change between two consecutive interferograms is larger than one interference phase value of typically 203.6 nm. This happens during large earthquakes when ground motion is too fast so that the fluid level of the

135   instrument cannot follow fast and large seismic surface wave arrivals in the first minutes.

B) SG:

– Correction of steps (offsets) of known origin (maintenance, liquid Helium refill)

– Removing disturbances (due to e.g. earthquakes), despiking and filling small gaps by applying PRETERNA (Wenzel, 1994).

140 – Decimation to 1 h samples after applying the numerical FIR filter g1m1h (http://www.eas.slu.edu/GGP/ggpfilters.html) which are then subject of the tidal analysis in order to adjust a local tidal model including the ocean tide loading effect. The tidal analyses are applied to high-pass filtered time series using the numerical FIR zero phase filter n60m60m2 (Wenzel, 1996) in order to remove all low-frequency signals including instrumental drift.

– Removing body and ocean tide loading based on the results of tidal analyses by applying ETERNA v3.4 and ETERNA-x

145   et34-x-v80 (Wenzel, 1996; Schüller, 2020), which provide accurate local tide models in the diurnal, semi-diurnal, ter-diurnal and higher frequency bands. Tidal parameters of theoretical body tide models (e.g. Dehant et al., 1999) are used for long-period tides.

– Removing the air pressure effect:

A) Tilt sensors:

150 – Applying the single admittance concept using air pressure admittances derived from tidal analyses in the tidal frequency band.

B) SG:

– Combining the prediction of operational 3D weather models (Klügel and Wziontek, 2009) and an additional single admittance correction which overcomes the limited temporal/spatial resolution of global weather models (Meurers et

155   al., 2013). Air pressure admittances derived from tidal analyses in the tidal frequency band have been used for this purpose.

– Removing the pole motion effect based on IERS earth rotation data (http://hpiers.obspm.fr/eop-pc/index.php) (SG only).

– Removing low order polynomial trend from the tilt data. The gravity time series is almost drift-free as proven by regular co-located absolute gravity measurements.

4 Local tide models and air pressure admittance

160

The local tide model for gravity matches the theoretical body tide models (e.g. Dehant et al., 1999; Mathews, 2001) and the ocean tide loading predictions provided by Bos and Scherneck (2017) almost perfectly (e.g. CSR4.0 (Eanes 1994), GOT00.2 (Ray 1999), TPXO7.2, TPXO9 (Egbert and Erofeeva 2002), FES2004 (Lyard et al. 2006), EOT11a (Savcenko and Bosch 2011), DTU10 (Cheng and Andersen 2010), HAMTIDE (Taguchi et al. 2014) and NAO99 (Matsumoto et al. 2000)). This is

165 due to the high accuracy of both the SG scale factor determination (0.2 %) at CO (Meurers, 2018a) and the tidal analysis, which is based on time series longer than 10 yr (Meurers, 2018b). The formal errors of gravimetric factors are far below 0.1 ‰ for the main tidal constituents. The RMS error of a single observation estimated from the residuals, which were calculated by using the adjusted tidal parameters, is 0.6 nm/s^2 or 0.2 ‰ of the tidal peak-to-peak amplitude only.

Local tide models for the tilt sensors are much less accurate. The RMS errors of a single observation range to 2.4 – 2.9 nrad

170 which is in the order of about 5 % of the peak-to-peak tidal signal. Also, much less data could be used for tidal analyses. Table 1 compares the tidal parameters of the main tidal groups for the LTS and iWT tilt sensors. The LTS N-S component turns out to be heavily disturbed by non-tidal excitation, particularly in the diurnal band, while the E-W components are not too far away from the body tide predictions. We also analyzed the data a-priori corrected for atmospheric and induced non-tidal oceanic loading contributions (Boy et al., 2009) provided by EOST loading Service (http://loading.u-strasbg.fr/).

175 However, the anomaly in the diurnal band still persists. A similar situation was reported already in the Michelson and Gale experiment in 1919 (Michelson and Gale, 1919; Ruotsalainen, 2018). However at CO, ocean loading corrections based on the TPXO9 model (http://holt.oso.chalmers.se/loading/) do not essentially reduce the deviation of observed tilt-factors from the body tide predictions. Because the tunnel axis is oriented in E-W direction, the N-S component corresponds to the tilt perpendicular to the tunnel axis and therefore is extremely sensitive to cavity effects (Harrison, 1976; Agnew, 1986). This is

180 the most likely reason for anomalous tidal parameters in N-S tilt, particularly in the diurnal band where N-S tilt wave amplitudes are small (<5 nrad). The high LTS/iWT ratio of the E-W tilt factors hints to calibration errors. LTS tilt factors are by 6–11 % higher than those of the iWT, i.e. the tidal parameters are probably affected also by unknown transfer functions of the tilt sensors. In order to consider all these problems properly, sensor dependent tidal models have been used for the tilt residual determination.

185 Air pressure has also a strong impact on observed tilts dominantly due to surface loading (e.g. Rabbel and Zschau, 1995). Air pressure admittances for tidal frequencies were calculated in a joint adjustment together with the tidal parameters by ETERNA-x et34-x-v80 software (Schüller, 2020). The results in Table 2 represent the diurnal and semidiurnal frequency band because long-period tides were not included in the adjustment. We also investigated the frequency dependence of the air pressure admittance by applying cross spectral analysis (Bendat and Piersol, 2010) on several detided tilt time series

190 covering intervals between 2 and 21 days (10 days on average), both for LTS N-S (Fig. 2) and LTS E-W.

For LTS N-S, the air pressure admittances confirm the number resulting from the tidal analysis (Table 2) obtained in the diurnal and semidiurnal frequency band. Clear time variability is seen obviously related to maintenance work (Fig. 2). In

May and September 2018 factory repairs by the manufacturer were necessary after thunderstorm strikes, partly damaging some electronic parts inside the sensor box. Before the LTS repair in May 2018, both admittance and phase increase slightly towards higher frequencies up to 0.3 mHz in all time series. Beyond about 0.3 mHz the admittance increase gets much stronger before it drops down at about 3–4 mHz. Note that the admittance functions are not corrected for the unknown transfer functions of the involved sensors. After the first repair, the admittance gets flat or even decreases already at frequencies >0.3 mHz. With very few exceptions, coherence is between 0.6 and 0.8 at frequencies <0.1 mHz for all LTS N-S time series and drops down to 0.3 to 0.4 at higher frequencies. The coherence decreases to less than 0.1 already between 0.1 mHz and 1 mHz after repair in May 2018. The picture is much less clear for LTS E-W. Coherence is at a very low level of 0.1–0.2 at all frequencies indicating that generally no or little dependence on air pressure exists as also suggested by Table 2. Nevertheless, we see a similar admittance change related to sensor maintenance as for LTS N-S.

Tilt meters are very sensitive to temperature changes. Klügel (2003) revealed instrumental effects of LTS tilt meters and interpreted them as being caused by quasi-adiabatic temperature changes associated with rapid air pressure variations. For the LTS tilt meters at CO, the temperature coefficient estimated from disturbances during maintenance work in the tunnel range from 3.9 to 4.9 µrad/K (LTS N-S) and 3.0 to 4.0 µrad/K (LTS E-W). Typically, fast air pressure changes caused by convective meteorological events amount up to 3 hPa. Klügel (2003) estimates the temperature variation due to air pressure change at 1.5 mK/hPa. Assuming this number to be valid also for the LTS tilt meter at CO, air pressure change of 1 hPa translates into a temperature variation up to 4.5 mK and consequently into about 7 nrad tilt. This corresponds to the air pressure admittance at about 0.3 mHz for N-S tilt (Fig. 2). The temperature change itself is below the recording resolution of the LTS temperature sensor (0.01 K). Therefore we did not directly observe temperature signals related to fast air pressure changes. A temperature sensor operating close to the end of the tunnel with 2 mK resolution since mid of 2018 indicates indeed a relation between air pressure and temperature increase. However, the currently available data do not allow quantitative analysis. The faster the air pressure changes the higher the frequency of the air pressure signal. This might be the reason for the admittance increase towards higher frequencies observed before the repairs.

Figure 3 proves that admittance function changes over time are of instrumental origin concerning either the tilt or the air pressure sensor or even both. We show the temporal variation of admittances and phases at 4 selected frequencies calculated with air pressure data acquired by the in-built sensor (LTS, Fig. 3, bottom panels) and the air pressure sensor of the SG (Fig. 3, middle panels) respectively. In addition, we present the temporal admittance function changes of the two pressure sensors (Fig. 3, top panels). A rapid but steady change happens between March and August 2017. The installation of the thermal insulation in August 2017 did obviously not affect the admittance function. However, after repair in May 2018, a sudden change of admittance and phase is visible at frequencies larger than 0.1 mHz which is probably related to the maintenance work. The described events appear synchronously in both air pressure to tilt admittance functions independent of the pressure sensor used for evaluation. This suggests that tilt signals with frequencies >0.3 mHz are of instrumental origin or at least strongly affected by instrumental issues, i.e. separating physically meaningful signals from instrumental artefacts is not

Hydrology and
Earth System
Sciences
Discussions

Open Access

EGU

possible in this frequency range. However, at long periods the air pressure signal in the tilt meter time series is due to geophysical/geodynamical reasons which are probably dominated by deformation due to air pressure loading. Here, the admittance is much higher for N-S tilt than for E-W tilt (see also Table 2) as expected due to the cavity effect. We come back

230   to this in chapter 5.1 when we discuss the direct Newtonian acceleration due to water mass load on the terrain surface.

5 Gravity and tilt residuals at Conrad Observatory

Figure 4 presents the final gravity and tilt residuals of the common observation period extending from end of April 2016 until mid of November 2018. Comparing the residuals with cumulative rain and snow (water equivalent) shows an obvious link between both short- and long-term residual anomalies and hydrological processes.

235   ### 5.1 Short-term signatures

Figure 5 presents a typical example of a heavy rain event on July 11, 2016. The SG residuals decrease sharply and exactly at the time when rain starts. This is mainly due to the Newtonian effect of rainwater distributed over the terrain surface. The gravity residual drop can be very well estimated by multiplying the cumulative rain with a rain admittance factor based on a digital terrain model in high spatial resolution (Meurers et al., 2007). The rain admittance depends on terrain geometry,

240   sensor location and on the area of rainwater accumulation. At CO, the rain admittance varies between -0.26 nm/s^2 and -0.29 nm/s^2 per 1 mm rain for accumulation areas between 10^4 and 10^2 km^2 (Fig. 6, left panel). Correcting for the Newtonian effect of cumulative rain removes the gravity response to rain almost perfectly (Fig. 5, light red line).

The same approach can be applied for estimating the Newtonian tilt effect of rain water both in N-S and E-W direction. Corresponding rain admittances turn out to be as small as $-1.3 \cdot 10^{-3}$ nrad per 1 mm rain for N-S tilt and $-7.6 \cdot 10^{-3}$ nrad per 1

245   mm rain for E-W tilt respectively, if the rain fall area extends to more than 2 km symmetrically around the tilt sensor (Fig. 6, right panel). In case of a rain front the Newtonian effect can be considerably larger depending on the direction from which the rain front approaches the station. The maximum estimate is provided by the effect of asymmetric rainfall areas extending to a line just passing the sensor location and does not exceed $\pm 7.7 \cdot 10^{-2}$ nrad per 1 mm rain at CO. However, in realistic weather situations, the rain to tilt admittance is much smaller and depends on the velocity at which the rain front moves over

250   the sensor. Given these small numbers, the Newtonian tilt effect of rain water turns out to be negligible at CO, because it does never emerge from the noise.

Nevertheless, there is a clear and instantaneous N-S tilt response on rain (Fig. 5). Tilt response on air pressure changes can be ruled out to be the reason in this case because the time patterns of air pressure and tilt are totally different, while tilt and cumulative rain match each other. Similar as in case of gravity, we do not observe any time delay between cumulative rain

255   and tilt response. In contrast, tilts in E-W direction rarely show short-term signatures that could be related to rain. In only 10 out of 48 rain events a slight residual depression is visible, which, however, often starts much earlier than rain.

Figure 7 shows the observed total N-S tilt offsets as function of cumulative rain or the surface pressure load exerted by cumulative rain at the end of the respective rain event. The rain admittance results to 0.73 nrad/mm. The observed rain admittance is about 580 times larger than the value estimated for pure Newtonian tilt (Fig. 6). It is about 7.4 nrad/hPa after

260 converting cumulative rain into surface load pressure. This corresponds to the air pressure admittance for the N-S tilt at about 0.3 mHz. The weak air pressure admittance for the E-W sensors may explain why we rarely see E-W tilt effects due to rain. The short-term N-S tilt response is therefore interpretable as pure deformation effect (strain induced tilt) due to surface load, which is probably enhanced by the cavity effect.

Figure 8 presents the gravity and tilt response of pure snow accumulation. Disdrometer data (coloured dots) show that almost

265 no liquid precipitation is involved. Note that rain gauges often report solid precipitation incorrectly and/or delayed in time. The disdrometer detects precipitation starting as snow grains and light drizzle during night and early morning with an intensity which is too small to be observed by the rain gauge. Precipitation continues as light to heavy snow from 8 a.m. onwards. The snow scale indicates the onset of snow cover increase at about 12 a.m. Gravity residuals start decreasing at the same time and reach a local minimum at about 10 p.m. when heavy snow fall terminates. The prediction of the cumulative

270 precipitation effect by applying the rain admittance concept follows the residual drop almost perfectly (Fig. 8, light red line). A significant signal associated with the main snow accumulation phase is also visible in the N-S tilt residuals, comparable in magnitude to rain fall events (compare to Fig. 5). Snow water equivalent matches the tilt time pattern if properly scaled (Fig. 8, orange line). Also in this case, gravity and tilt react instantaneously i.e. without time delay. Obviously no essential water infiltration can take place because most precipitation is solid. Therefore, deformation due to surface loading rather than due

275 to pore pressure changes explains the observed short-term tilt signal.

5.2 Long-term signatures

After rainfall, a slow discharge process brings the gravity residuals back to their initial level in most cases (Fig. 4). However, in some events the residuals exceed the initial level remarkably, in particular after long-lasting rain or rapid snowmelt. We interpret this as response to downwards water flow (infiltration) from terrain surface into the ground until water is stored

280 somewhere below the SG sensor. This process probably starts as soon as the subsurface is sufficiently saturated by rain or snowmelt water and therefore needs a certain threshold to be triggered. Mangou (2019) estimated that about 20 mm water accumulation within the past 3 days is required. However, this number is a rough estimate. The hydrological charge and discharge history as well as meteorological conditions (e.g. evaporation rate etc.) play a role as well. There are a few candidates for water storage volumes at CO:

285 − the gravel layer below the concrete base plate of the underground observatory building and the laboratories in front of the tunnel,

− fissures and cracks in the solid rock or

− eventually a karstic volume filled by water after heavy rain/snowmelt.

All events of this kind are marked by vertical dotted lines in Fig. 4. Interestingly, all of them are associated with

290 simultaneous tilt anomalies: Almost at the same time when the SG residual starts to increase, we see a strong signal in the tilt time series as well. N-S tilt shows always a steep residual drop, the E-W tilt residuals (in particular LTS) temporarily increase but with much less amplitude. Therefore E-W tilt signals are often masked by noise. Tilt residuals reach their extreme in advance compared to gravity. Figure 9 exemplarily zooms into a long-lasting rain event (Fig. 9, left panel) and into a rapid snowmelt event (Fig. 9, right panel). N-S and E-W tilts reach their extremes almost at same time but 1-2 days

295 earlier than the gravity residuals do. Later, residuals return to their former level; a process which takes about 14 days or more.

6. Discussion and Conclusion

Comparing the E-W and N-S tilt data, the amplitude ratio of which is ~0.1 on average, a clear systematic tendency of the source azimuth (340° to 350°) is indicated. Based on the high resolution digital terrain model of the area (Meurers et al.,

300 2007) the existence of any surface depression capable to cumulate run-off water mass (Kalmár and Benedek, 2018) enough for generating the observed tilts can be checked. Although there is a valley, the deepest point of which is nearly in this direction, its distance from the sensors is too large as Fig. 10 shows. Moreover, from Fig. 10 one may conclude that enormous water mass (equivalent to 1000 m^3) should be accumulated somewhere near to the surface in the very close vicinity (< 50 m) of the observatory to produce purely gravitational tilt even for a fraction of the observed one. It means that

305 100 mm rain fallen on 1 km^2 should be somehow caught to a compact reservoir to obtain 5 nrad tilt. However, there is no any evidence of such a large basin or cavity next to CO. This estimation is based on forward gravitational modelling of the horizontal attraction of mass columns (e.g. Papp and Benedek, 2000) representing the water mass placed on the top of the topographic mass columns. The N-S and E-W tilt effects τ of 10 mm water height were computed at sensor location for each mass column selected by the azimuth and then the uniform water volumes of 25 m^3 (50 m × 50 m × 0.01 m) were scaled by

310 the ratio 1/τ.

Regarding the long-term residual variations a pure Newtonian effect of one single source (e.g. one karstic cave filled by water) representing the water accumulation at a specific location somewhere in the sensors' surroundings can be ruled out due to two reasons:

− model calculations show that no reasonable solution exists to explain the observed tilt and gravity effects and

315 − the onsets of the residual features in gravity and tilt do not coincide exactly in time.

Herbst (1979) reports tilt signals in the period range of several days obtained from Askania borehole tilt meter measurements in Zellerfeld-Mühlenhöhe (Germany) which occurred at precipitation events or during snowmelt periods. The observed long-term tilt response is very similar in shape and amplitude to the observations at CO (Fig. 4). Different model calculations ruled out thermoelastic disturbances in the surrounding rock due to temperature changes or resulting from heat transfer by

320 the rain/snowmelt water. Instead, Herbst (1979) explained the tilt response by lateral fluctuations in the fracture water level inducing pressure differences in adjacent fracture systems, which consequently cause elastic bending of rock structures.

Active pumping or injection experiments at different spatial scale have proven high sensitivity of tilt to pore pressure changes (Weise, 1992, Kümpel et al., 1996; Weise et al. 1999, Fujimori et al. 2001, Jahr et al. 2008, Jahr et al. 2018). In a large-scale injection experiment at the KTB deep drilling site (Germany) Jahr et al. (2006a, 2006b, 2008) studied the surface

325 deformation due fluid induced stress changes by borehole tilt meter array observations. They detected tilt signals with magnitudes between 450 nrad and 700 nrad after three months of water injection and interpreted the observations as deformation effect caused by the induced pore-pressure change, whereby deformation extends from the upper crust to the surface.

Additionally, this study showed that the tilt response to precipitation or ground water level variations differed from station to

330 station within the array (Jahr et al., 2006a; Jahr et al., 2006b). Only one of in total five tilt records reflects a strong response to heavy rain events. The associated long-term signatures at this site are very similar to those observed at CO, both in shape and magnitude. Jahr et al. (2009) analyzed high resolution tilt observations at the Geodynamic Observatory Moxa (Germany) revealing a strong correlation of tilt signals with ground water level changes. Their study proves again that pore pressure changes due to water content variations in the subsurface, e.g. as result of precipitation or ground water level variations, are

335 able to induce tilt.

Due to the high sensitivity and extremely low and linear instrumental drift of SG sensors the SG gravity residuals reveal very clearly the Newtonian effect (vertical component) of water mass transport involved in hydrological charge and discharge processes. Certainly, the hydrological water transport process is very complex at CO. Contrary; the tilt meters are not able to capture the gravitational effect because it is hidden in the noise. However, in particular the N-S tilt residuals show significant

340 both short- and long-term anomalies, which are associated with the same rain or snowmelt events and are clearly related to the residual patterns captured by the SG gravity record. Therefore we explain the tilt residual anomalies by strain-tilt coupling effects due to surface or subsurface deformation. Here we can distinguish two hydrological processes:

– Charge process: Deformation caused by surface load (rain water, snow) produces short-term tilt anomalies associated with heavy precipitation.

345 – Discharge process: Deformation probably caused by pore pressure changes in the adjacent fracture system induces long-term tilt anomalies lasting over up to 3 weeks.

In both cases, tilts in N-S direction are enhanced due to the cavity effect. It is not the physical source, but the hydrological process, which links the residual anomalies of gravity and tilt. Presently, it is not yet clear, if karstic phenomena play an important role at CO as well. No large caves are known in the rock massif the CO is located on. However, we cannot exclude

350 that deformation by internal loading could take place, e.g. when an eventually existing cave system would be filled by water during hydrological discharge.

Hydrology and
Earth System
Sciences
Discussions

Code and Data availability. ETERNA-x et34-x-v80: http://ggp.bkg.bund.de/eterna/; ETERNAv3.4: International Center for Earth Tides, https://webdevel.upf.pf/ICET/home.html; TSOFT: Royal Observatory of
355 Belgium, http://seismologie.oma.be/en/downloads/tsoft; gravity data: International Geodynamics and Earth Tide Service (IGETS), http://igets.u-strasbg.fr/; tilt data are available on request.

Author contributions. Tilt meter set-up and maintenance: GP, JB, HR, RL; SG maintenance: RL with co-workers, BM; processing of tilt data: GP, JB; processing of the gravity data: BM; tidal analyses and cross spectral analysis: BM; final residuals: BM, GP; data analyses: BM, GP, JB; interpretation and discussion of results: all authors; paper writing: BM with
360 contributions from all authors.

Competing interests. The authors declare that they have no conflict of interest.

370 **References**

Agnew, D.C.: Strainmeters and tiltmeters. Review of Geophysics, 24, 579-624, 1986.

Bendat, J.S. and Piersol, A.G.: Random Data: Analysis and Measurement Procedures, John Wiley and Sons, New York, 602 p., 2010.

Blaumoser, N.: Hydrological and geological investigations at Trafelberg mountain, Cobs-Journal 2011, 12
375 http://www.conrad-observatory.at/zamg/index.php/de/downloads-de/category/5-cobsjournal, 2011.

Bonaccorso, A., Falzone, G. and Gambino, S.: An investigation into shallow borehole tiltmeters, Geoph. Res. Lett., 26/11, 1637-1640, https://doi.org/10.1029/1999GL900310, 1999.

Bos, M.S. and Scherneck, H.G.: Free ocean tide loading provider, Available at: http://holt.oso.chalmers.se/loading/, last access: 21 December 2017.

380 Boy, J.-P., Longuevergne, L., Boudin, F., Jacob, T., Lyard, F., Llubes, M., Florsch, N. and Esnoult, M.F.: Modelling atmospheric and induced non-tidal oceanic loading contributions to surface gravity and tilt measurements, J. Geodyn., 48:182-188, 2009.

Bryda, G. and Posch-Trözmüller, G.: Geological investigation of the drill core from borehole TB2A: First results. CobsJournal 2014-2015, 9, http://www.conrad-observatory.at/zamg/index.php/de/downloads-de/category/5-cobsjournal, 2015.

Cheng, Y. and Andersen, O.B.: Improvement in global ocean tide model in shallow water regions, in: Proceedings of the OSTST Meeting, Lisbon, Portugal, 18-22 October 2010, 2010.

Crossley, D., Hinderer, J., Casula, G., Francis, O., Hsu, H.T., Imanishi, Y., Jentzsch, G., Kääriänen, J., Merriam, J., Meurers, B., Neumeyer, J., Richter, B., Shibuya, K., Sato, T. and van Dam, T.: Network of Superconducting Gravimeters Benefits a Number of Disciplines, EOS, Transactions, AGU, 80, No. 11, 125-126, 1999.

Crossley, D., Calvo, M., Rosat, S. and Hinderer, J.: More Thoughts on AG–SG Comparisons and SG Scale Factor Determinations, Pure Appl. Geophys., 175, 1699-1725, https://doi.org/10.1007/s00024-018-1834-9, 2018.

Dehant, V., Defraigne, P. and Wahr, J.M.: Tides for a convective Earth, Jour. Geoph. Res., 104, 1035-1058, 1999.

Deisl, S., Blaumoser, N. and Leonhardt, R.: Hydrology and Geology at the Trafelberg, Cobs Journal 2012-2013, http://www.conrad-observatory.at/zamg/index.php/de/downloads-de/category/5-cobsjournal#, 2013.

Eanes, R.J.: Diurnal and semidiurnal tides from TOPEX/POSEIDON altimetry, EOS, Trans. Am. Geoph. Un., 75(16), 108, 1994.

Egbert, G.D. and Erofeeva, L.: Efficient inverse modeling of barotropic ocean tides, J. Atmos. Oceanic Technol., 19(2), 183-204, 2002.

Fujimori, K., Ishii, H., Mukai, A., Nakao, S., Matsumoto, S. and Hirata, Y.: Strain and tilt changes measured during a water injection experiment at the Nojima Fault zone, Japan, The Island Arc, 10, 228-234, https://doi.org/10.1111/j.1440-1738.2001.00320.x, 2001.

Goodkind, J.M.: The superconducting gravimeter, Rev. Sci. Inst., 70/11, 4131-4152. https://doi.org/10.1063/1.1150092, 1999.

Harrison, J.C.: Cavity and topographic effects in tilt and strain measurements, Jour. Geoph. Res., 81, 319–328, 1976.

Harrison, J.C. and Herbst, K.: Thermoelastic strains and tilts revised, Geoph. Res. Lett., 4/11, 535-537, https://doi.org/10.1029/GL004i011p00535, 1977.

Hartmann, H. and Hartmann, W.: Die Höhlen Niederösterreichs, vol. 5, Wissenschaftliche Beihefte zur Zeitschrift "Die Höhle," 54, Landesverein für Höhlenkunde in Wien und Niederösterreich, Wien (Eds.). 2000.

Herbst, K.: Interpretation of Tilt Measurements in the Period Range Above that of the Tides, Terrestrial Sciences Division, Project 7600, Air Force Geophysics Laboratory, 89 pp, https://books.google.at/books?id=vBkotgEACAAJ, 1979.

Hinderer, J., Crossley, D. and Warburton, R.: Superconducting gravimetry. In: Herring, T. and Schubert, G. (Eds.), Treatise on Geophysics, vol. 3, Geodesy, Elsevier, 65-122, 2007.

Jahr, T.: Non-tidal tilt and strain signals recorded at the Geodynamic Observatory Moxa, Thuringia/Germany, Geodesy and Geodynamics, 9, 3, 229-236, https://doi.org/10.1016/j.geog.2017.03.015, 2018.

13

Jahr, T., Letz, H. and Jentzsch, G.: Monitoring fluid induced deformation of the earth's crust: A large scale experiment at the KTB location/Germany, Jour. Geodyn., 41/1-3, 190-197, https://doi.org/10.1016/j.jog.2005.08.003, 2006a.

Jahr, T., Jentzsch, G. and Gebauer, A.: Observations of fluid induced deformation of the upper crust of the Earth: Investigations about the large scale injection experiment at the KTB site/Germany, Bull. d'Inf. Mar. Terr., 141, 11271-11275,
420   2006b.

Jahr, T., Jentzsch, G., Gebauer, A. and Lau, T.: Deformation, seismicity, and fluids: Results of the 2004/2005 water injection experiment at the KTB/Germany, Jour. Geoph. Res., 113, B11410, doi:10.1029/2008JB005610, 2008.

Jahr, T., Jentzsch, G. and Weise, A.: Natural and man-made induced hydrological signals, detected by high resolution tilt observations at the Geodynamic Observatory Moxa/Germany, Jour. Geodyn., 48/3, 126-131, 2009.

425   Kalmár, J. and Benedek, J.: Determination of water load and catchment lines by the modeling of infiltration and run-off of rain water (in Hungarian), Dimenziók: Matematikai Közlemények, 5, 25-29, 2018.

Klügel, T.: Bestimmung lokaler Einflüsse in den Zeitreihen inertialer Rotationssensoren (LOK - ROT), Schlussbericht, DFG-Forschungsprojekt LOK-ROT (SCHR 645/1), Wettzell, https://www.yumpu.com/de/document/view/12632682/lok-rot-geodatisches-observatorium-wettzell, 2003.

430   Klügel, T. and Wziontek, H.: Correcting gravimeters and tilt meters for atmospheric mass attraction using operational weather models. Jour. Geodyn., 48, 204-210, https://doi.org/10.1016/j.jog.2009.09.010, 2009.

Kümpel, H.J., Varga, P., Lehmann, K. and Mentes, G.: Ground tilt induced by pumping - preliminary results from the Nagycenk test site, Hungary, Acta Geod. et Geoph. Hungary, 91(1-2), 67-78, 1996.

Lyard, F., Lèfevre, F., Letellier, T. and Francis, O.: Modelling the global ocean tides: a modern insight from FES2004,
435   Ocean Dyn., 56, 394-415, 2006.

Mathews, P.M.: Love numbers and gravimetric factor for diurnal tides, in: Proceedings of the 14th International Symposium on Earth Tides, Jour. Geod. Soc. Japan, 47/1, 231-236, 2001.

Mangou, S.: Response of tilt and gravity on environmental processes at Conrad observatory, Austria, Msc thesis, University of Vienna, 89 pp., 2019.

440   Matsumoto, K., Takanezawa, T. and Ooe, M.: Ocean tide models developed by assimilating TOPEX/POSEIDON altimeter data into hydrodynamical model: a global model and a regional model around Japan. Jour. Oceanography, 56, 567-581, 2000.

Meurers, B.: Superconducting Gravimeter Calibration by CoLocated Gravity Observations: Results from GWR C025, Int. Jour. Geoph., Volume 2012 (2012), Article ID 954271, 12 pages, https://doi.org/10.1155/2012/954271, 2012.

445   Meurers, B.: Scintrex CG5 used for superconducting gravimeter calibration, Geod. and Geodyn., 9/3, 197-203, https://doi.org/10.1016/j.geog.2017.02.009, 2018a.

Meurers, B.: 10 years SG gravity time series at Conrad Observatory (Austria) - Station report, 1st Workshop on the International Geodynamics and Earth Tide Service (IGETS), 18-20 June 2018, Potsdam, Germany, http://igets.u-strasbg.fr/2018workshop/1.2_03_CO.pdf, 2018b.

450 Meurers, B., Van Camp, M. and Petermans, T.: Correcting superconducting gravity time-series using rainfall modelling at the Vienna and Membach stations and application to Earth tide analysis, Jour. Geod., 81/11, 703-712, https://doi.org/10.1007/s00190-007-0137-1, 2007.

Meurers, B., Dorninger, M., Mikolaj, M. and Blaumoser, N.: Results and comparison of gravity time series at Vienna and Conrad observatory, 17th International Symposium on Earth Tides, 15-19 April 2013, Warsaw, Poland, 2013.

455 Meurers, B., Van Camp, M., Francis, O. and Pálinkáš, V.: Temporal variation of tidal parameters in superconducting gravimeter time-series, Geoph. Jour. Int., 205/1, 284-300, https://doi.org/10.1093/gji/ggw017, 2016.

Michelson, A.A. and Gale, H.: The rigidity of the Earth. Astrophys. Jour., 50, 330-345, 1919.

Mikolaj, M. and Meurers, B.: Hydrology Induced Gravity Variation Observed at Vienna and Conrad Observatory, Geoph. Res. Abstr., 15, EGU2013-6003, EGU General Assembly 2013, Vienna, Austria, 07-12 April
460 2013, https://meetingorganizer.copernicus.org/EGU2013/EGU2013-6003.pdf, 2013.

Papp, G. and Benedek, J.: Numerical modeling of gravitational field lines - the effect of mass attraction on horizontal coordinates, Jour. Geod., 73. 648-659, 2000.

Papp, G., Ruotsalainen, H., Meurers, B., Leonhardt, R., Benedek, J., Hutchinson, P. and Szántó, M.: Analysis of Environmental and Loading Effects in Tilt and SG Gravity Observations at Conrad (Austria) and Peters Seismological
465 (Australia) Observatories, IUGG-G06l, 27th IUGG General Assembly, 8-18 July 2019, Montréal, Québec, Canada, 2019.

Ray, R.D.: A global ocean tide Model from TOPEX/POSEIDON Altimetry: GOT99.2, NASA Technical Memorandum 209478, 1999.

Rabbel, W. and Zschau, J.: Static deformations and gravity changes at the earth's surface due to atmospheric loading, Jour. Geoph, 56, 81-99, 1995.

470 Ruotsalainen, H.: Interferometric Water Level Tilt Meter Development in Finland and Comparison with Combined Earth Tide and Ocean Loading Models, Pure Appl. Geoph., 175, 1659-1667, https://doi.org/10.1007/s00024-017-1562-6, 2018.

Ruotsalainen, H., Bán, D., Papp, G., Leonhardt, R. and Benedek, J.: Interferometric Water Level Tilt Meter at the Conrad Observatory. COBS Journal 2014-2015, 11, http://www.conrad-observatory.at/zamg/index.php/de/downloads-de/category/5-cobsjournal#, 2016a.

475 Ruotsalainen, H., Papp, G., Leonhardt, R., Bán, D., Szűcs, E. and Benedek, J.: Comparison of broad band time series recorded by FGI type interferometric water level- and Lippmann's pendulum type tilt meters recording parallel at Conrad observatory, Austria. Geoph. Res. Abstr., 18, EGU2016-6932, EGU General Assembly 2017, 23-28 April 2017, Vienna, Austria, 2016b.

Savcenko, R. and Bosch, W.: EOT11a - a new tide model from multimission altimetry, in: Proceedings of the OSTST
480 Meeting, 19-21 October 2011, San Diego, USA, 2011.

Schüller, K.: Program System ETERNA-x et34-x-v80-* for Earth and Ocean Tides Analysis and Prediction, Documentation Manual 01: Theory, Surin, Thailand, January 2020, 209 pp., 2020.

Taguchi, E., Stammer, D. and Zahel, W.: Inferring deep ocean tidal energy dissipation from the global high-resolution data-assimilative HAMTIDE model, Jour. Geoph. Res. Oceans,119, 4573-4592, doi:10.1002/2013JC009766, 2014.

485   Van Camp, M. and Vauterin, P.: Tsoft: graphical and interactive software for the analysis of time series and Earth tides, Comp. Geosc., 31/5, 631-640, 2005.

Voigt, C., Förste, C., Wziontek, H., Crossley, D., Meurers, B., Pálinkáš, V., Hinderer, J., Boy, J.-P., Barriot, J.-P. and Sun, H.: Report on the Data Base of the International Geodynamics and Earth Tide Service (IGETS), (Scientific Technical Report STR – Data; 16/08), Potsdam: GFZ German Research Centre for Geosciences, DOI: http://doi.org/10.2312/GFZ.b103-490   16087, 2016.

Weise, A.: Neigungsmessungen in der Geodynamik - Ergebnisse von der 3-Komponentenstation Metsahovi, PhD Thesis (in German), Technical University of Clausthal, Germany. 180 p., 1992.

Weise, A., Jentzsch, G., Kiviniemi, A. and Kääriäinen, J.: Comparison of long period tilt measurements: Results from two clinometric stations Metsähovi and Lohja, Finland, Jour. Geodyn., 27, 237-257. 1999.

495   Wenzel, H.G.: PRETERNA - a preprocessor for digitally recorded tidal data, Bull. d'Inf. Mar. Terr., 118, 8722-8734, 1994.

Wenzel, H.G.: The Nanogal Software: Earth Tide Data Processing Package ETERNA 3.30, Bull. d'Inf. Mar. Terr., 124, 9425-9439, 1996.
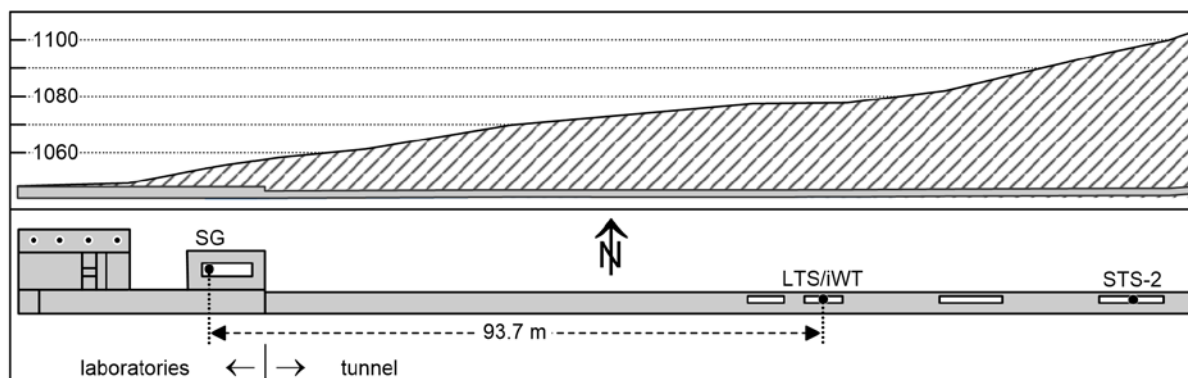
500   **Figure 1: Vertical section (height in [m]) and ground plan of the Conrad observatory. Sensor positions are displayed by black dots. Small dots indicate boreholes of different depth.**
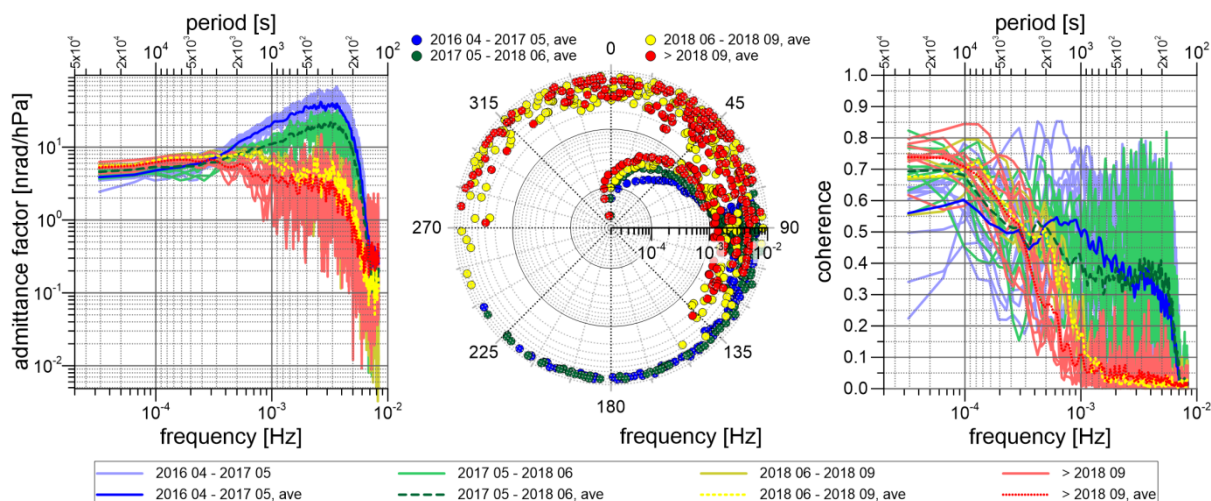
Figure 2: Air pressure admittance function of the LTS/N-S tilt sensor derived from different observation periods covering a few days to less than 3 weeks each. Admittance (left), phase (middle), coherence (right). Circles and lines with intensive colors show the admittance (left), phase (middle) and coherence (right) respectively, averaged over the time series within 4 intervals (beginning - May 2017; May 2017 - June 2018/LTS repair; June 2018 - September 2018/LTS repair; September 2018 - end).
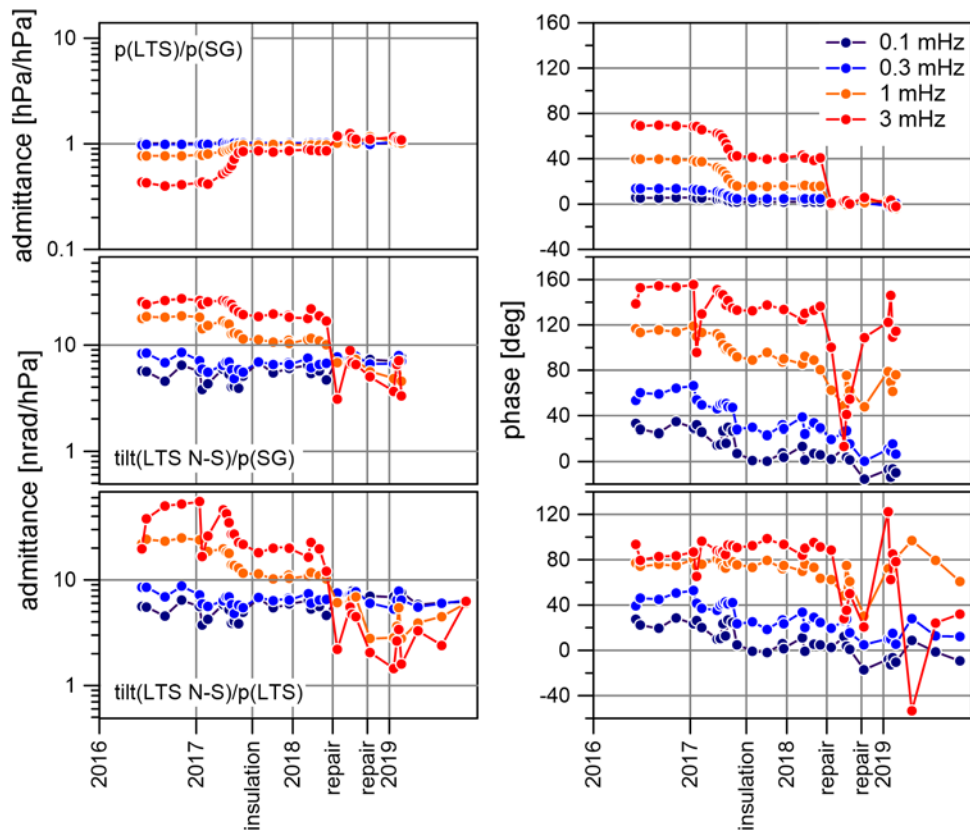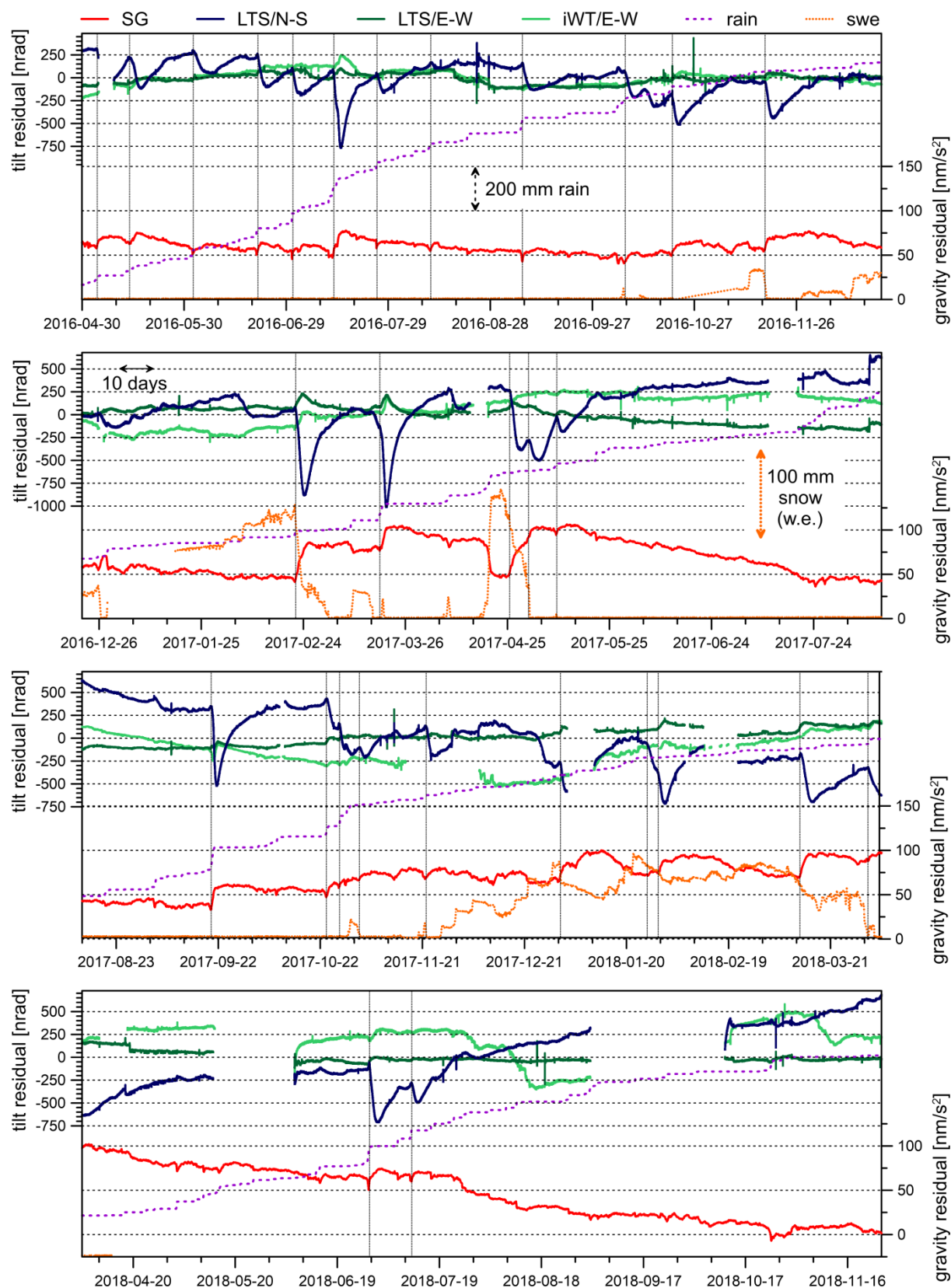
Figure 3: Air pressure to tilt (N-S) admittance function and their temporal evolution at selected frequencies using data from different air pressure sensors (bottom: LTS air pressure sensor; middle: SG air pressure sensor). The top panel shows the SG to LTS air pressure admittance function.

510 **Figure 4: Comparison of gravity and tilt residuals: gravity (red, bottom), tilt N-S (LTS, dark blue, top), tilt E-W (LTS: dark green, iWT: light green), cumulative rain (dotted purple line); snow water equivalent (dotted orange line). Scales for rain and snow (water equivalent) are indicated by arrows. Vertical dotted lines mark the onset of hydrological long-term events.**
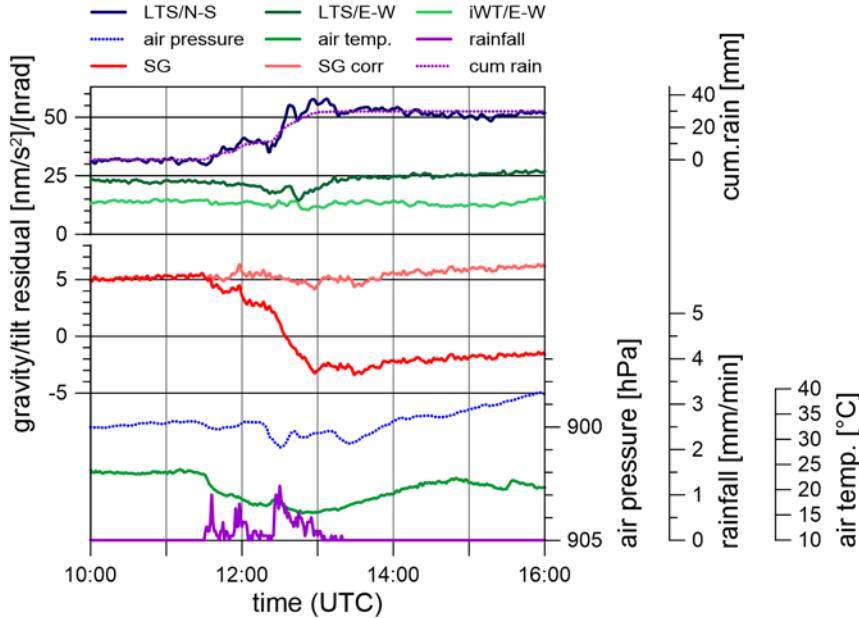
Figure 5: Effect of heavy rain on gravity and tilt at CO on July 11, 2016. Gravity and N-S tilt residuals show patterns clearly related to cumulative rain, while E-W tilts do not or only weakly respond to rain. Top: N-S tilt residuals (dark
515 **blue), E-W tilt residuals (LTS/dark green and iWT/light green), cumulative rain (dotted purple line) scaled to fit the N-S tilt optimally. Middle: SG gravity residuals (red), gravity corrected for cumulative precipitation (light red). Bottom: rainfall (purple), air pressure (dotted blue line) and outdoor air temperature (green).**
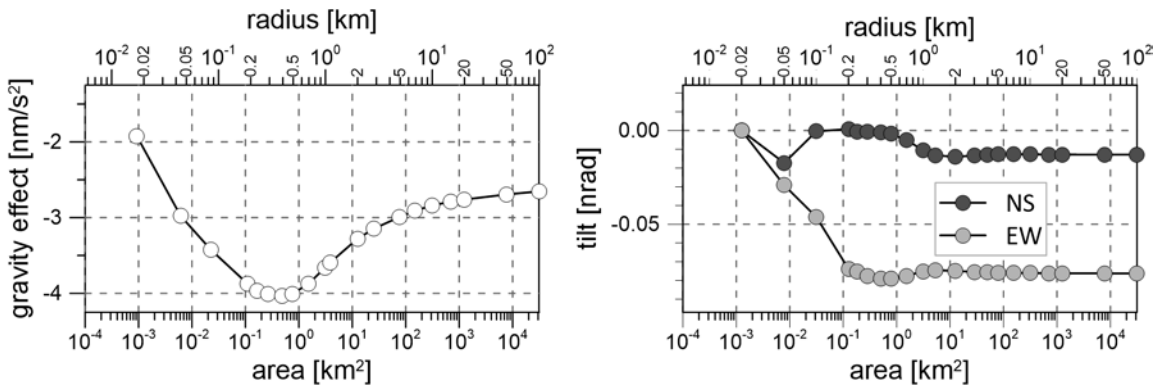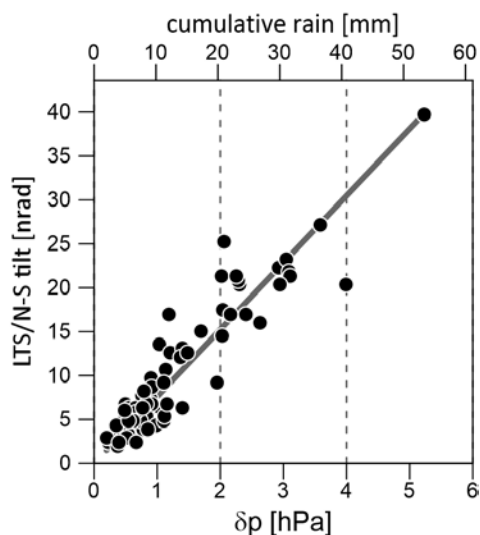

Figure 6: Gravitational effect of 10 mm rain on gravity (left) and tilt (right) at CO.

Figure 7: N-S tilt response on cumulative rain at CO. Converting cumulative rain to surface pressure load reveals tilt to pressure admittance of 7.6 nrad/hPa (solid line).
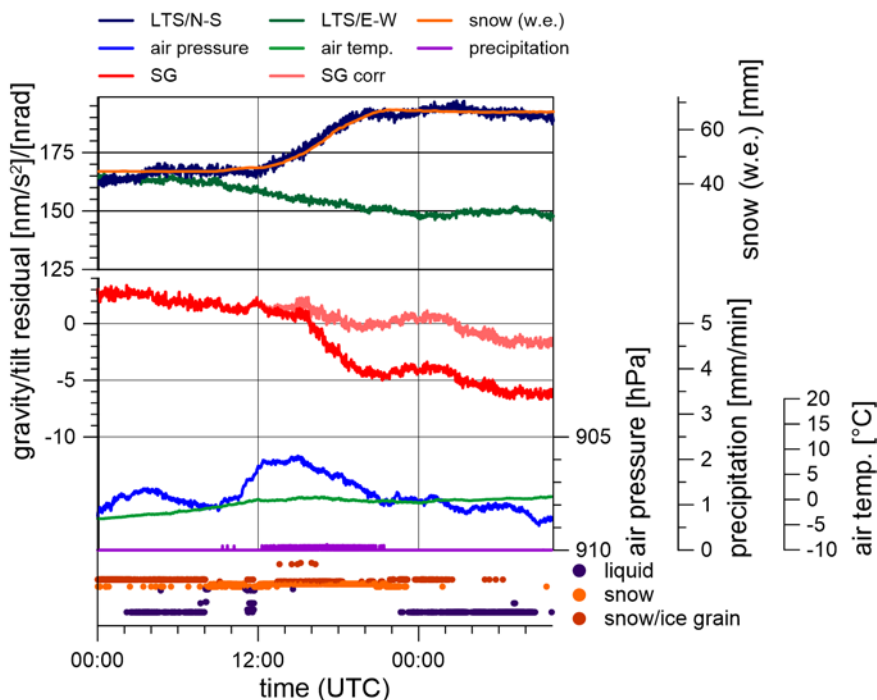

Figure 8: Effect of snow accumulation on gravity and tilt at CO on December 21 and 22, 2017. Top: N-S tilt residuals (dark blue), E-W tilt residuals (dark green), snow (water equivalent, orange) scaled to fit the N-S tilt optimally. Middle: SG gravity residuals (red), gravity corrected for cumulative precipitation (light red). Bottom: air pressure (blue) and outdoor air temperature (green).
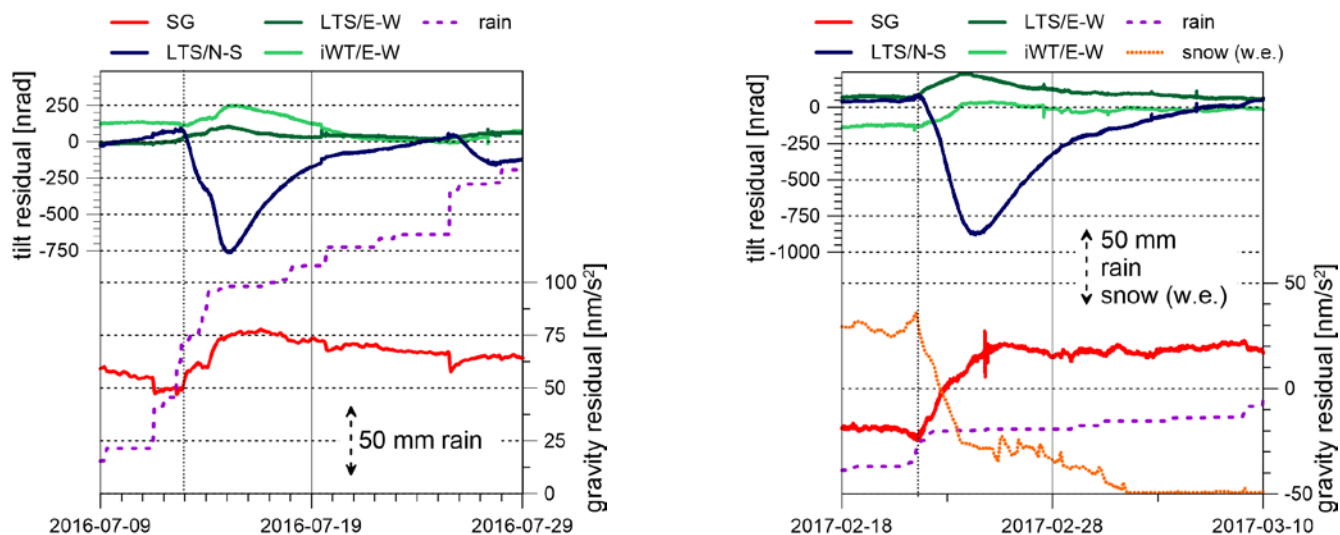
Figure 9: Long-term gravity and tilt residual signals caused by hydrological processes after heavy and long-lasting rain (left panel)
and during rapid snowmelt (right panel). Top: N-S tilt residuals (dark blue), E-W tilt residuals (dark green and light green).
Bottom: SG gravity residuals (red). Cumulative rain (dashed purple line), snow (water equivalent, dotted orange line); scales for
rain and snow w.e. indicated by arrows.
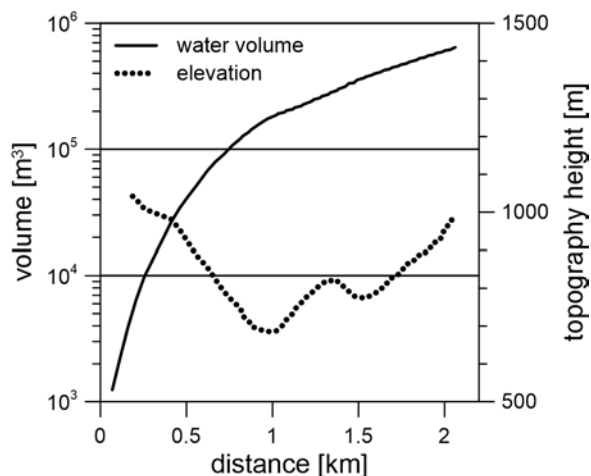
Figure 10: Estimation of the magnitude of water volume (black) capable to produce 1 nrad tilt if it was purely Newtonian. The
dotted line shows the cross section of the topography in the specific azimuth (about 350°) defined by the E-W and N-S tilts detected
during rainfall events.

		N-S			E-W					$\frac{\gamma(LTS)}{\gamma(iWT)}$
		LTS-Y				LTS-X		iWT-X		
Darwin	γ (WD)	amp [nrad]	γ σ(γ)	φ[°] σ(φ)	amp [nrad]	γ σ(γ)	φ[°] σ(φ)	γ σ(γ)	φ[°] σ(φ)	
O1	0.6944	3.1275	1.0997 0.0358	7.235 1.867	23.4455	0.7135 0.0034	-6.902 0.272	0.6746 0.0058	-11.349 0.493	1.0577
K1	0.7362	4.3962	1.2920 0.0259	-1.318 1.152	32.9605	0.7773 0.0026	-7.615 0.187	0.7278 0.0040	-11.244 0.314	1.0680
N2	0.6911	7.3013	0.6648 0.0067	-2.691 0.579	9.8359	0.7673 0.0039	-2.495 0.288	0.7130 0.0048	-4.449 0.382	1.0762
M2	0.6911	38.1330	0.6628 0.0013	-3.193 0.115	51.3708	0.7401 0.0015	-4.102 0.060	0.6849 0.0010	-5.525 0.080	1.0806
S2	0.6911	17.7398	0.6777 0.0031	-2.880 0.264	23.8984	0.6896 0.0018	-2.676 0.146	0.6203 0.0023	-5.015 0.204	1.1117
K2	0.6911	4.8195	0.6612 0.0129	-2.531 1.116	6.4926	0.6880 0.0073	-2.577 0.608	0.6385 0.0097	-4.875 0.871	1.0775

Table 1: Comparison of tidal parameters derived from tilt time series at CO

Air pressure admittance [nrad/hPa]		
N-S	E-W	
LTS-Y	LTS-X	iWT-X
4.247 ±0.034	0.097 ±0.019	-0.475 ±0.034

Table 2: Air pressure admittances in the diurnal and semidiurnal frequency band for the tilt sensors derived from tidal analysis.